catalysts

MDPI

Article

Direct One-Step Seedless Hydrothermal Growth of ZnO Nanostructures on Zinc: Primary Study for Photocatalytic Roof Development for Rainwater Purification

Marie Le Pivert [1,2], Aurélie Piebourg [1], Stéphane Bastide [3], Myriam Duc [4] and Yamin Leprince-Wang [1,*]

[1] ESYCOM Lab, CNRS, Université Gustave Eiffel, F-77454 Marne-la-Vallée, France
[2] COSYS/ISME Lab, IFSTTAR, Université Gustave Eiffel, F-77447 Marne-la-Vallée, France
[3] ICMPE, UMR 7182 CNRS, Université Paris-Est Créteil, F-94320 Thiais, France
[4] GERS/SRO, IFSTTAR, Université Gustave Eiffel, F-77447 Marne-la-Vallée, France
* Correspondence: yamin.leprince@univ-eiffel.fr

Abstract: To shift towards the greener city, photocatalytic urban infrastructures have emerged as a promising solution for pollution remediation. To reach this goal, the large bandgap semiconductors, such as nontoxic Zinc Oxide (ZnO), already proved their excellent photocatalytic performances. However, integrating and developing cost-effective and greener photocatalytic surfaces with an easily scaled-up synthesis method and without energy and chemical product overconsumption is still challenging. Therefore, this work proposes to develop a depolluting Zinc (Zn) roof covered by ZnO nanostructures (NSs) using a one-step seedless hydrothermal growth method in 2 h. The feasibility of this synthesis was firstly studied on small areas of Zn (1.25 cm^2) before being scaled up to medium-sized areas (25 cm^2). The efficiency of this functionalization route for ZnO NSs grown without seed layer was attributed to the presence of Zn^{2+} sites and the native oxide film on the Zn surface. Their photocatalytic efficiency was demonstrated by removing in less than 3 h the Methylene Blue (MB) and Acid Red 14 (AR14) in both DI water and rainwater under UV-light. Promising results were also recorded under solar light. Therefore, the photocatalytic Zn roof functionalized by ZnO NSs is a promising route for rainwater purification by photocatalysis.

Keywords: photocatalysis; water purification; ZnO nanostructures; hydrothermal synthesis; seedless; building materials

Citation: Le Pivert, M.; Piebourg, A.; Bastide, S.; Duc, M.; Leprince-Wang, Y. Direct One-Step Seedless Hydrothermal Growth of ZnO Nanostructures on Zinc: Primary Study for Photocatalytic Roof Development for Rainwater Purification. *Catalysts* **2022**, *12*, 1231. https://doi.org/10.3390/catal12101231

Academic Editor: John Vakros

Received: 16 July 2022
Accepted: 11 October 2022
Published: 14 October 2022

1. Introduction

Access to water poses a growing risk to the economy as well as to the communities and ecosystems that depend on it. Fresh water is indeed a limited resource whose direct consumption is restricted and could be affected by pollution and contamination. It is therefore more important than ever to preserve easily accessible fresh water sources such as rainwater. Nevertheless, the quality of rainwater is affected by polluted air [1], i.e., it naturally contains some pollutants present in the atmosphere [2]. Hence, some pollutants are drawn from the atmosphere to the ground during rainy days. At this stage, the concentration of pollutants is extremely low, but it continues to increase as the water passes through the urban environment to the wastewater treatment plants. As a result, rainwater affects at the same time, the soil, the groundwater, the human health and the ecosystem. It is therefore essential to reflect upon direct rainwater treatment in urban areas.

As a green and sustainable method of environmental pollution remediation, photocatalytic processes are being studied extensively as possible air and water treatments due to their ability to remove refractory pollutants at different scales and places without requiring complex and expensive infrastructures [3,4]. They are particularly attractive and suitable for this type of treatment because they could use only solar energy (inexhaustible) and a photocatalyst, which is mostly a wide bandgap metal oxide semiconductor. Moreover, they

do not require the handling of expensive chemicals and can be operated autonomously to mineralize micropollutants into CO_2, H_2O, and other light by-products [4].

Therefore, the development of photocatalytic urban infrastructures has emerged as a promising solution to address environmental pollution directly near emission sources, thereby avoiding pollutant accumulation and dispersion in urban areas [5–7]. To develop these infrastructures, large bandgap semiconductors, such as nanostructured dioxide titanium (TiO_2) and zinc oxide (ZnO), were mainly used and already proved their excellent photocatalytic performance at the laboratory scale [2,5–9]. For these materials to be highly efficient, they must be elaborated as nanostructures (NSs) owing a high volume-to-surface ratio, in order to develop a very large free active area [10]. The production pathway should be short (few hours) and easily scale-up, using the less energy and chemical products to be the as green as possible. Efforts are still being made to develop this kind of synthesis method to produce large-scale surface. To the best of our knowledge, photocatalytic urban infrastructures are currently produced by incorporating nanoparticles in civil engineering materials [11,12], such as concrete or paint; by depositing a semiconductor layer on the surface [12]; or recently by growing ZnO NSs on the urban infrastructures by two-step hydrothermal synthesis [13,14]. This last process has the advantage to functionalize the civil engineering material surface in less than 2 h and consumes few energy and chemical products. Nevertheless, it requires a ZnO seed layer deposition and double annealing at 350 °C. In order to optimize the synthesis process and to make it greener, an improved ZnO NSs synthesis method will be studied by choosing the appropriate substrate allowing a surface functionalization with only one step instead of two steps.

Therefore, to manage rainwater directly at the first source of runoff with ecofriendly photocatalytic urban infrastructures, this work proposes to develop a depolluting Zinc (Zn) roof covered with ZnO NSs using a one-step seedless hydrothermal growth method in 2 h to produce a large surface of 5 cm × 5 cm. Zinc is indeed a material commonly used in new construction buildings, which allows the use of hydrothermal synthesis in the absence of the seed layer deposition step, thus avoiding the overconsumption of energy and chemical products. Moreover, ZnO is nontoxic, biocompatible, and inexpensive in terms of raw materials, making it a remarkable large bandgap photocatalyst. First, the feasibility of a cost-effective and environmentally compatible production of this photocatalytic surface was studied, as well as the use of a post-annealing treatment. Samples were thoroughly characterized by scanning electron microscopy (SEM FEG ZEISS Merlin, Oberkochen, Germany) to investigate the morphology of the ZnO NSs, by X-ray diffraction (XRD, Brucker Advance) using a cobalt anticathode for the study of the microstructures, by UV–visible spectrophotometry for ZnO bandgap determination (UV-visible, Maya2000 Pro from Ocean Optics, Duiven, Netherlands) and for absorbance measurements of the organic dyes (Perkin Elmer Lambda 35, Waltham, MA, USA) to monitor their degradation, and by photoluminescence (PL) to obtain more information concerning defects both in as-grown and annealed ZnO samples. Then, the photocatalyst properties of both sample types were evaluated with respect to the removal of Methylene Blue (MB) and Acid Red 14 (AR14) in DI water and in rainwater under UV-light and natural solar light. Finally, the synthesis was scaled-up to produce a 5 cm × 5 cm ZnO/Zn roof surface in order to simulate on a small-scale the behavior of rainwater on this surface under artificial solar light illumination.

2. Results

2.1. Characterization of ZnO Nanostructures Grown on Zn Surface

To evaluate the production of ZnO NSs based photocatalytic surfaces by one-step seedless hydrothermal synthesis, the functionalization process was firstly developed on a small scale flattened Zn wires (2.5 cm × 0.5 cm), as shown in Figure 1a. Functionalized Zn samples, both as grown (ZnO/Zn(AG)) and post-annealed (ZnO/Zn, 30 min at 350 °C), exhibited ZnO bandgap values similar to those grown on silicon or on tiling substrates by the classical two-step hydrothermal growth (Figure 1b) [13,14]. No apparent difference was recorded between the UV-Vis spectra of the as-grown and annealed sample, with an average

ZnO bandgap of 3.20 ± 0.02 eV. Only a slight variation in intensity was recorded depending on the location of the measurement. Indeed, the surface of mechanically flattened Zn wire is not smooth, thereby affecting the light path during the acquisition of the UV-vis spectrum.

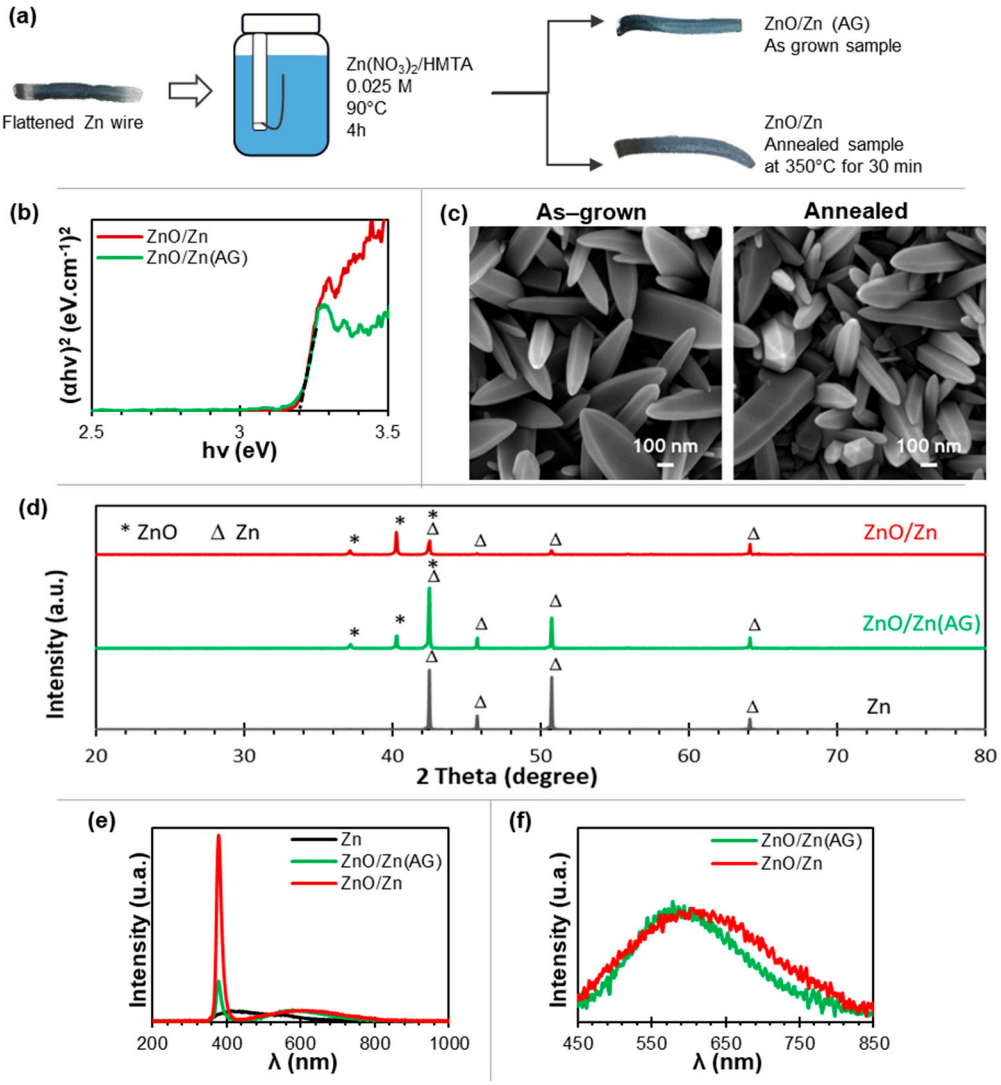

Figure 1. (**a**) Schematic of the experimental set-up for the synthesis of ZnO NSs on flattened Zn wires; (**b**) UV–visible spectral plots according to the Tauc-Lorentz model, (**c**) SEM images and (**d**) XRD patterns of ZnO/Zn(AG) and ZnO/Zn samples, (**e**) PL spectrum of ZnO/Zn(AG) and ZnO/Zn samples, (**f**) PL visible emission band of ZnO/Zn(AG) and ZnO/Zn samples.

The non-perfect homogeneity and the roughness of the Zn substrate surface resulted in some defects on the grown ZnO nanostructures. Nevertheless, the entire surface of the Zn wire was covered by the ZnO NSs (Figure 1c). Indeed, SEM images of ZnO NSs grown on Zn showed a high density of nanowires (NWs) and nanorods (NRs), as traditionally obtained by the hydrothermal route [15,16]. It should be noted that here the substrate is not the typical laboratory substrate, such as glass or silicon, with a well-defined planar surface. Therefore, the NWs/NRs are not perfectly vertical to the substrate and some other punctual NSs appeared.

Figure 1d shows the XRD diffractograms of the ZnO/Zn(AG) and ZnO/Zn samples where the two hexagonal crystal structures of Zn and ZnO can be clearly identified. The four peaks at 42.5°, 45.7°, 50.5°, and 64.2° correspond respectively to the (002), (100), (101), and (102) plan of Zn (reported values from ICDD N° 01-085-5877). Thus, these four peaks are related to the substrate used as clearly identified on the Figure 1d. The ZnO XRD

pattern correspond to the three main peaks of Würtzite ZnO, which are (100) at 37.2°, (002) at 40.3°, and (101) at 42.5° (reported values from ICDD N° 98-002-9272) [17,18]. An improvement in crystallinity related to the annealing post-treatment (350 °C) can be observed from the XRD patterns: the intensity of the ZnO peaks increased while the intensity of the Zn peaks decreased. The XRD patterns and SEM images show a preferential growth direction of the ZnO NSs along the c-axis ([0001] direction of the hexagonal structure).

The crystallinity improvement induced the post-treatment at 350 °C during 30 min were also observed by PL measurements (Figure 1e). Indeed, an increase of the UV emission band; related to near band-edge transition, namely the free exciton recombination through an excition-excition collision process; and a slight decrease of visible emission band; related to defect levels, such as Zn_i, V_O, and O_i; were conjointly recorded on ZnO/Zn compared to ZnO/Zn(AG) spectrum. This trend was attributed to the improvement in crystallinity. Moreover, by examine the visible emission band, a red-shift in the peak position was recorded after the annealing treatment (Figure 1f). This shift may due to the deep level defects, such as V_O and O_i, which were usually observed in the oxygen-rich sample giving orange-red emission [19].

After obtaining on small Zn samples with ZnO NSs showing good morphological and textural characteristics despite the absence of both pretreatment and seedlayer coating, the suitability of large-scale synthesis was evaluated by functionalizing a flat Zn sheet (5 cm × 5 cm, sampled from a commercial Zn roof—Leroy Merlin, Collégien, France) (Figure 2a). At this scale, the presence of ZnO NSs on the substrate is accompanied by a slight whitish coloration of the sheet. As expected, the as-grown functionalized Zn sheet, ZnO/Zn(AG), exhibits similar ZnO bandgap values to those obtained at a smaller scale, with an average at 3.21 ± 0.01 eV (Figure 2b).

SEM observations revealed a sligthly different ZnO nanostructure with longer and thinner NWs (Figure 2c), which could be caused by the different nature of the substrate: the Zn wires used in the small-sample experiments has only a native oxide film, while the Zn roof material has been laminated and treated chemically by the manufacturer to form a protective layer containing alkaline Zn carbonate ($2\ ZnCO_3 \cdot 3\ Zn(OH)_2$) on the Zn surface. Moreover, the Zn sheet has the advantage to be more smooth than above used wires avoiding irregularity during the growth. This result is consistent with the literature, where hydrothermal scaled-up synthesis on silicon wafer has already been demonstrated [20,21]. Furthermore, a shorter growth time, 2 h instead of 4 h, was also tested to determine its influence on the characteristics of ZnO NWs. SEM images showed that smaller NWs are obtained but with a lager areal density for 2 h: ~35 NWs/μm^2 vs. ~15 NWs/μm^2, for 4 h-sample.

Figure 2d shows the XRD diffractograms of the ZnO/Zn(AG) samples obtained after 4 h and 2 h synthesis, as well as that of the bare Zn roof substrate. On the ZnO/Zn(AG) roof samples, the two hexagonal crystal structures of Zn and ZnO are clearly identified with no significant difference between the 4 h and 2 h samples. As previously, on the wire samples, the Zn XRD pattern is related to the Zn substrate used. Meanwhile, the ZnO XRD patterns correspond to the typical XRD patterns of the ZnO Würtzite phase.

The similarity between ZnO/Zn(AG) 4 h and ZnO/Zn(AG) 2 h were also observed on the PL spectrum with no shift of UV or visible emission bands (Figure 2e,f). Only a slight difference of intensity, with more intense peaks for ZnO/Zn(AG) 4 h, were recorded. The increase of intensity may be due to the growing amount of ZnO with the hydrothermal duration. Moreover, in accordance with our results, previous PL analysis works showed an increasing intensity in the visible emission band with the growth time, which was mainly attributed to the change of the concentration of the structural defects in the ZnO nanowires [22].

It should be emphasized that the absence of post-treatment (as-grown samples) is tested with the aim of developing a future application. In this way, it is in principle possible to save the energy consumed by a post-annealing (350 °C, 30 min), while a shorter growth time would be advantageous to increase the production rate of photocatalytic roofs. Of course, these savings will be meaningful only if good photocatalytic performances are verified.

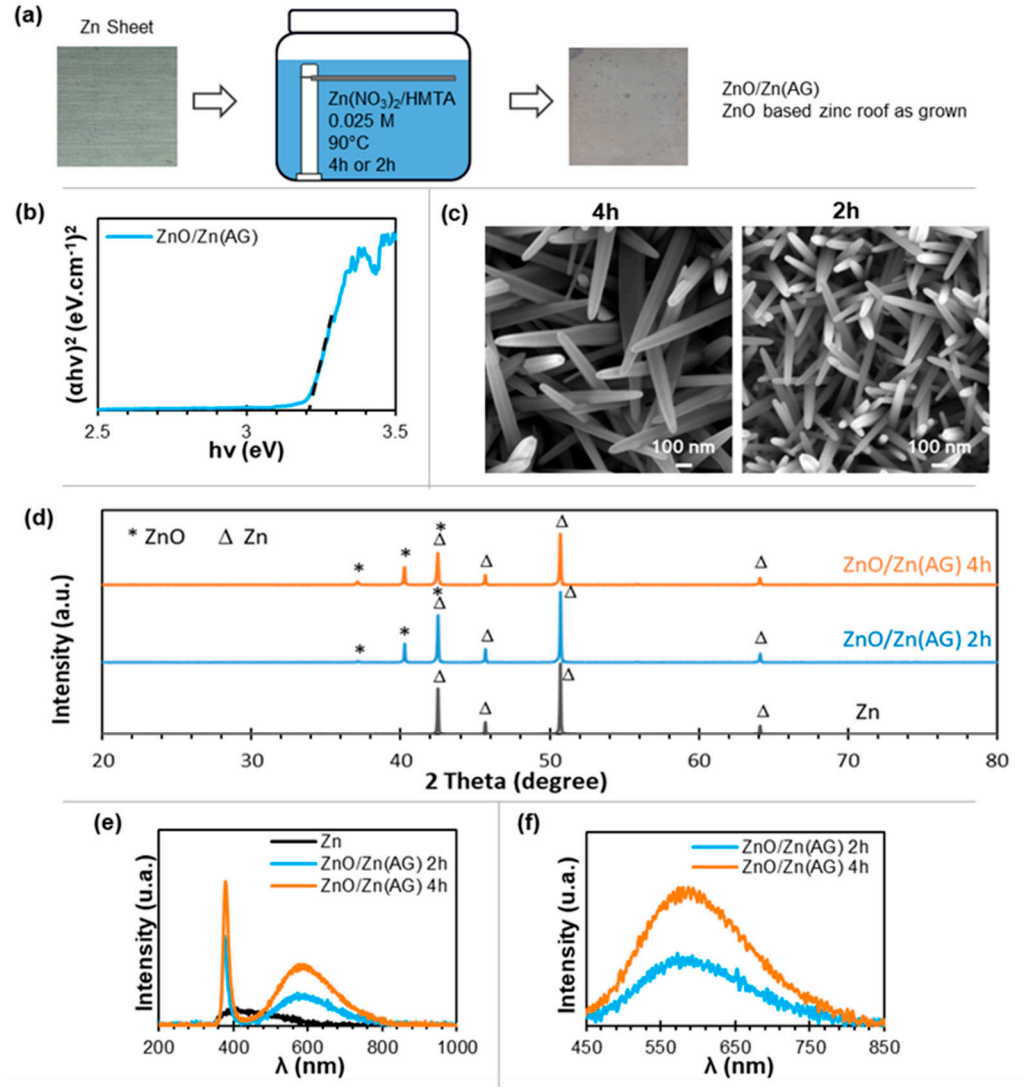

Figure 2. (**a**) Schematic of the experimental set-up for the synthesis of ZnO NSs on Zn roof sheets; (**b**) UV–visible spectral plots according to the Tauc-Lorentz model, (**c**) SEM images and (**d**) XRD patterns of ZnO/Zn(AG) samples grown for 4 h or 2 h, (**e**) PL spectrum of ZnO/Zn(AG) samples grown for 4 h or 2 h, (**f**) PL visible emission band of ZnO/Zn(AG) samples grown for 4 h or 2 h.

2.2. Photocatalytic Activity Evaluation

2.2.1. Methylene Blue Photodegradation under UV-Light

To test the photocatalytic activity of ZnO NSs on flattened Zn wires under reproducible conditions, the photodegradation of MB in DI water was first studied under a powerful UV-light source (Hamamatsu LC-8, ~365 nm, ~35 mW/cm^2). Results demonstrated that ZnO NSs lead to a total degradation in less than 120 min against 71% after 180 min for photolysis performed without ZnO (Figure 3a). Comparing these results with those obtained previously with larger substrates [13], ZnO NSs grown on flattened Zn wires seem to provide a good surface area/efficiency ratio. This means that good photocatalytic activity was recorded for ZnO/Zn(AG) and ZnO/Zn. No significant difference was observed between the as-grown and post-annealed samples, with only a slight improvement in the efficiency of ZnO/Zn compared to ZnO/Zn(AG). Taking this into account, the ZnO/Zn(AG) photocatalyst (the most eco-compatible option) appears to be the best choice for treating polluted rainwater via a functionalized Zn roof.

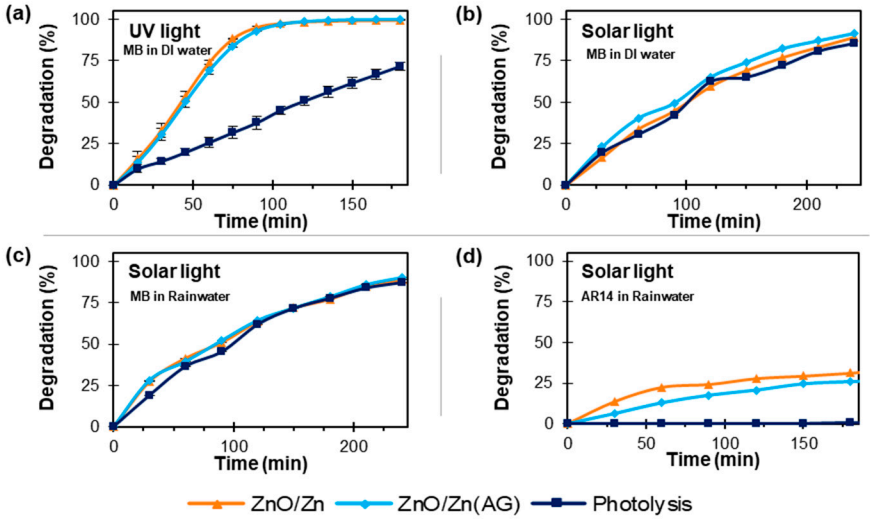

Figure 3. MB photodegradagtion with and without ZnO NSs under (**a**) UV light source (~365 nm, 35 mW/cm^2) in DI Water, (**b**) natural solar light (April/May, France, I_{UV} = 2.3 mW/cm^2) in DI Water, and (**c**) natural solar light (April/May, France, I_{UV} = 2.3 mW/cm^2) in rainwater; (**d**) AR14 photodegradation with and without ZnO NSs under natural solar light (April/May, France, I_{UV} = 2.9 mW/cm^2) in rainwater.

2.2.2. Photodegradation of Methylene Blue under Natural Solar Light

In order to evaluate the photocatalytic activity of nanostructured ZnO under conditions closed to the reality, tests were performed in April/May in Paris, France under natural solar light, whose UV part of the spectrum corresponds to ~2.3 mW/cm^2. The results (Figure 3b) showed that the use of ZnO NSs grown on flattened Zn wires improves the photodegradation of MB very slightly compared to natural photolysis. The same observation was made in a previous work and explained in that MB is very easy to degrade under solar light [14].

Chemical stability and possible competition in terms of photodegradation with other media-specific species were evaluated with the same experiments done in rainwater instead of DI water. Rainwater is known to have a slightly acidic pH and to contain a number of micro-pollutants whose presence could affect the MB removal process due to side reactions, competition at the surface of the photocatalyst, and partial poisoning of the active sites by chemicals present in rainwater. A comparison between Figure 3b,c, however, shows that none of these effects are observed, as the degradation rates are similar in both media. In fact, the easy photolysis degradation of MB can mask the photocatalytic contribution.

2.2.3. Photodegradation of Acid Red 14 in Rainwater under Natural Solar Light

To extend the evaluation of the photocatalytic performance of nanostructured ZnO, another organic dye, AR14, which is more resistant than MB to natural solar light was chosen for a photodegradation test [14]. This test was carried out in rainwater under cloudy weather, as previously, the efficiency of ZnO/Zn(AG) and ZnO/Zn was evaluated and compared to the photolysis in the same conditions. No photolysis was recorded under natural solar light, thereby allowing a better estimation of the photocatalytic activity of ZnO NSs (Figure 3d). Indeed, the photodegradation observed is only due to the photocatalytic activity of the roof functionalization. In contrast to the results under UV light, ZnO/Zn appears to be slightly more efficient than ZnO/Zn(AG) under natural solar light (Figure 3d).

2.2.4. Photodegration of Polluted Runoff Waters on ZnO/Zn Sheets under Solar Light

This section is a preliminary study to evaluate the relevance of ZnO/Zn(AG) development at large scale for the depollution of runoff waters using functionalized Zn roofs. An AR14 at a concentration of 10 µM in a rainwater solution was flowed over a ZnO/Zn(AG) sheet (5 cm × 5 cm, sampled from commercial Zn roof) under a solar lamp (Zolix, Sirius-

300P, Beijing, China, 300 W, 320–2500 nm) with a flow rate of 0.17–1.03 mL/min (Figure 4a). Only a single pass was carried out without recirculation of the treated water in order to simulate roof runoff conditions during rainy weather. Same experiments were carried out with a Zn sheet without functionalization treatment. Results with and without ZnO NSs were then compared to calculated an average gain corresponding to the deviation between the photolysis rate and the photocatalysis rate.

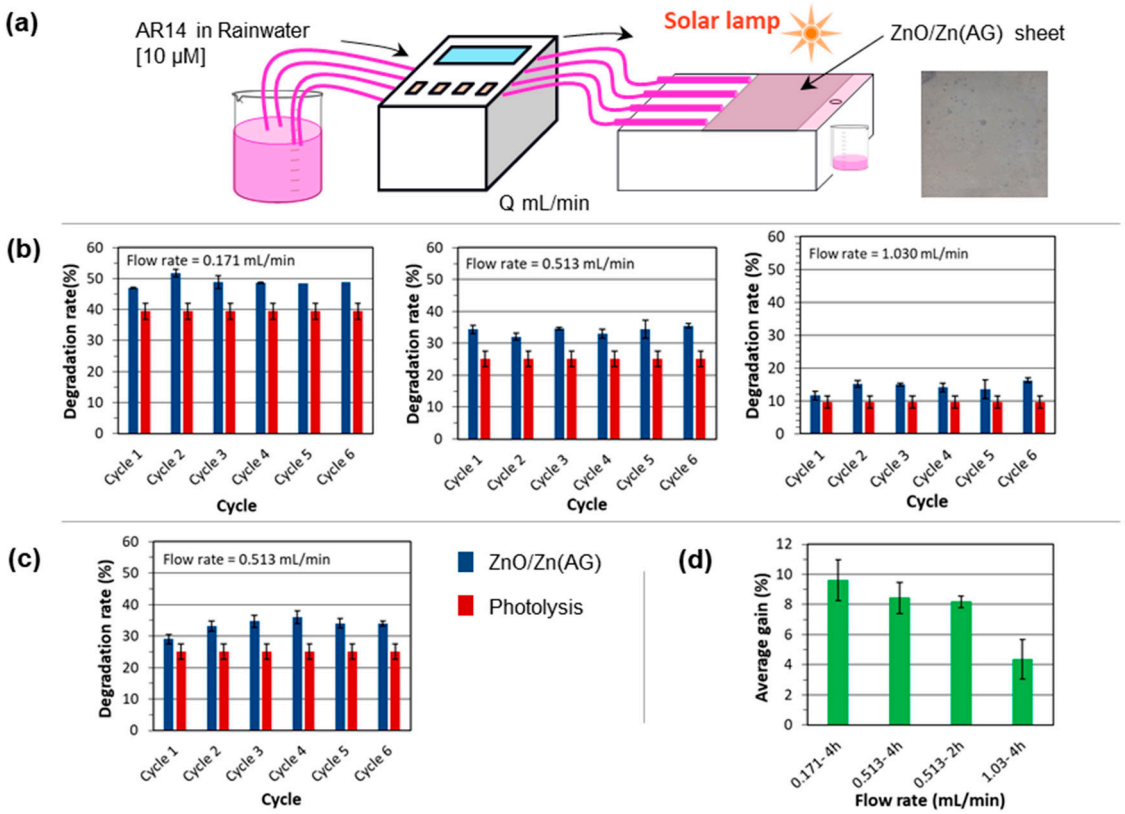

Figure 4. (**a**) Schematic of the experimental set-up of runoff water photodegradation with ZnO NSs on Zn roof sheets. Photodegradation rate of AR14 under artificial solar light with or without the presence of ZnO NSs: (**b**) at different flow rate: 0.171, 0.513, and 1.03 mL/min for 4 h-sample; (**c**) for 2 h-sample with a flow rate of 0.513 mL/min. (**d**) Comparison of the photocatalytic efficiencies for the different cases under studied.

The ZnO NSs average gain varied between 7% and 12% for a flow rate of 0.171 mL/min and between 6% and 9% for a flow rate of 0.513 mL/min, whereas the high flow rate of 1.03 mL/min resulted in a very low average gain of 2% to 6%. Coupled to this decrease of the average gain, the photodegradation rate decreases as the flow rate increases, which can be explained by the shorter residence time of the dye solution under the solar lamp.

For all flow rates, the ZnO/Zn(AG) stability was studied. The results shown in Figure 4b correspond to successive cycles of photocatalysis with a DI water rinse step followed by drying with a hot airflow stream and 15 min under solar lamp irradiation. These results show that there is no loss of efficiency during cycles 1 to 4. No loss of photocatalytic activity was also recorded between cycles 4 to 6, corresponding to consecutive cycles of photodegradation with only a short DI water rinse step followed by a drying with hot airflow. This observation was made in the case of all flow rates tested and supports the stability of the samples.

A comparative study between samples synthesized in 4 h and in 2 h was carried out. It aims at reducing the manufacturing cost for future photocatalytic roof applications. An intermediate flow rate of 0.513 mL/min was chosen for this test. At this flow rate, the degradation rates reported in Figure 4b (4 h-sample) and Figure 4c (2 h-sample) are very

close. The Figure 4d gives a comparative illustration of the four presented cases, which allows to conclude that the hydrothermal synthesis time of ZnO NSs can be reduced from 4 h to 2 h without loss in efficiency.

3. Discussion

3.1. ZnO Nanostructures Growth on Zinc Substrate

The characterization work (Figures 1 and 2) demonstrated that ZnO NSs could be grown on a Zn substrate by a one-step seedless hydrothermal growth method, although the route generally used to produce ZnO NSs on a substrate is a seeded growth on ZnO nanoparticles or film-coated substrate [23,24]. However, for some substrates, self-seeded technology or local surface properties allow the direct growth of ZnO NSs, as is the case for Zn substrates.

A first hypothesis that could explain this observation is the formation of a local seed layer on the substrate surface at the initial stage preceding the crystal growth. The Zn substrate can react with hydroxide ions produced in the synthesis solution to form soluble zincate ions ZnO_2^{2-}, which in turn can react with water to deposit a ZnO (solid phase) seed layer according to the following reactions [23–25]:

$$Zn + 2\,OH^- \rightarrow ZnO_2^{2-} + H_2 \quad (1)$$

$$ZnO_2^{2-} + H_2O \rightarrow ZnO + 2\,OH^- \quad (2)$$

This preformed ZnO layer on the Zn substrate has proven to be a crucial step for the successful nucleation and subsequent growth of ZnO NSs [24,25]. Therefore, after the local oxidation of Zn, ZnO NSs can grow directly on the substrate without phase matching problems, according to the classic hydrothermal mechanisms:

$$(CH_2)_6N_4 + 6\,H_2O \rightarrow 6\,HCHO + 4\,NH_3 \quad (3)$$

$$NH_3 + H_2O \rightarrow OH^- + NH_4^+ \quad (4)$$

$$Zn^{2+} + 4\,OH^- \rightarrow Zn(OH)_4^{2-} \rightarrow ZnO + 2\,OH^- + H_2O \quad (5)$$

$$Zn(NH_3)_4^{2+} + 2\,OH^- \rightarrow ZnO + 4\,NH_3 + H_2O \quad (6)$$

$$Zn^{2+} + 2\,OH^- \rightarrow Zn(OH)_2 \xrightarrow{\Delta} ZnO + H_2O \quad (7)$$

The second hypothesis, which can explain the growth of ZnO NSs without a seed layer, is also directly related to the species generated by the hydrothermal synthesis from reactions (3) and (4). Zn can react with NH_4^+ to form Zn^{2+} and other species (Equation (8)) [26]. Then Zn^{2+} can react with OH^- following Equation (7) to form ZnO. Therefore, at the initial growth stage, the Zn substrate acts as both a source of Zn^{2+} and of nucleation sites. Finally, after this initial stage, the hydrothermal growth process will follow the classic mechanisms for 4 h (reactions (3) to (7)). This process happens preferentially along the *c*-axis [0001] due to the minimum value of the (002) surface free energy (9.9 eV·nm^{-2}) compared to ones of different plans, such as (110) and (100) (12.3 and 20.9 eV·nm^{-2}, respectively), justifying the ZnO synthesis as NWs and NRs instead nanosheets or other morphologies.

$$Zn + 2\,NH_4^+ \rightarrow Zn^{2+} + 2\,NH_3 + H_2 \quad (8)$$

According to these two hypotheses, which may be valid conjointly, the participation of Zn on the substrate surface as a driving force occurs only during the initial phase. Indeed, after the formation of the first ZnO layers, Zn is protected and can no longer react directly with the solution [26], thus explaining the ZnO NSs well-synthesized as nanowires and nanorods after 4 h.

The results in Figure 2, demonstrating efficient up-scaling, imply that this method is applicable to the mass production of ZnO NSs-based roofs. This is in good agreement with

the literature, where hydrothermal synthesis has been shown to be effective in functionalizing large silicon wafers [20,21] and in producing a few square meters of ZnO NSs-based pavers for tiles and bitumen roads [27]. The one-step functionalization of Zn sheets is also consistent with previous work where Zn substrates were functionalized in a chemical bath solution at low temperature [25,28].

3.2. ZnO/Zn Photocatalytic Activity

The total photodegradation of MB within 3 h of light exposure demonstrates an excellent photocatalytic activity under UV light (Figure 3a) of both types of sample (as grown and annealed). By comparison, with the results obtained on large substrates tested under the same experimental conditions [13], it appears that a 1.25 cm^2 sample of ZnO NSs grown on Zn by the present method (one-step) develops the same photocatalytic activity as a 1.55 cm^2 sample of ZnO NSs grown onto silicon by the classical method (two-step). No significant difference was observed between as grown and annealed samples, due to the fact that the morphologies of ZnO NSs are similar (Figure 1c). Only a slight variation in kinetics could be recorded between the two types of samples due to the better crystallinity after post-annealing at 350 °C during 30 min (diffractograms in Figure 1d).

Under natural solar light, there is no real difference between photolysis and photocatalysis for MB removal due to its fairly easy degradation under illumination. The study of AR14 degradation reveals that the annealed sample performed slightly better than the as grown sample. The degradation rates under solar illumination are overall much lower than those under UV lamp illumination because natural solar light contains much less UV (~5%).

The ease of scale-up of this synthesis is already proved (Figure 2) and the suitability of ZnO/Zn(AG) to clean-up runoff water is promising given the stability of the photocatalytic activity over several water cycles (Figure 4). It is mentioned in the literature that after long rainfall (which corresponds to the case of successive cycles in our study), the photocatalytic surface tends to be saturated and a limit in the purification capacity can be reached [7]. Under these conditions, incomplete photodegradation leads to the adsorption of by-product on the ZnO surface, which results in an inhibition of the photocatalyst surface by blocking all active sites. Nevertheless, this was not the case in this work, even in the absence of sample regeneration. Comparing the degradation rates by photocatalysis and photolysis, it is possible to observe a small gain related to the presence of ZnO NSs under this condition, which could be largely improved by increasing the residence time under irradiation, but it will be against the real working conditions of the Zn roof application.

The photocatalytic degradation rate depends largely on the experimental conditions and the type of photocatalyst. Nevertheless, it is therefore important to put our results into perspective. An efficiency close to 70% for the degradation of MB (10 mM) was obtained with ZnO nanorods substrate (3 cm × 1 cm) in a PMMA cuvette under visible light irradiation (AM 1.5G, 1 $kW{\cdot}m^2$) from a solar simulator (SS1.6 kW from science tech, Canada) after 90 min [29]. Quartz cuvettes with 10 mL of MB (10 mM) and various ZnO NSs under four visible light lamps (20 W each) lead to a maximal degradation rate of 36.3% [30]. In borosilicate beakers, under solar light, MB at 100 µM and pH 3 was photodegraded in the presence of TiO_2 (0.5 g/L) and H_2O_2 (10 mM) at 92% after 3 h [31]. 48 mg of $ZnCo_2O_4/Co_3O_4$ was poured in AR14 solution (1.2 mg) leading to a photodegradation rate from 29% to 95% under solar illumination (125 W) depending on the photocatalyst synthesis method used [32]. TiO_2 nanopowders demonstrated a photodegradation rate range from 90% to 100% in 60 min under simulated solar light (7.7 $\mu W/cm^2$) for AR14 at 20 ppm [33].

4. Materials and Methods

4.1. ZnO Nanostructures Based Zinc Roof Synthesis and Characterization

Flattened Zn wire (2.5 cm × 0.5 cm) and Zn roof sheet (5 cm × 5 cm) were used as substrate for ZnO NSs growth by one-stage seedless hydrothermal synthesis. The samples were functionalized by the two different routes described below, before being carefully characterized by UV–visible spectroscopy (Maya2000 Pro from Ocean Optics,

IDIL, Orsay, France) and by field-emission scanning electron microscopy (SEM FEG ZEISS Merlin, Oberkochen, Germany) to determine their bandgap value and to investigate the morphology of the obtained ZnO nanostructures. Samples were also characterized by X-ray diffraction (Bruker Advance, Champs-sur-Marne, France) using a cobalt anticathode (λ = 1.78897 Å, 35 kV, 40 mA) and by photoluminescence (He-Cd Laser, IK Series, KIMMON, Laser Components, Meudon, France, λ = 325 nm, P = 10 mW).

4.1.1. ZnO/Zn Wires Production

Without any special washing process, the Zn wire substrates were directly functionalized by a one-step seedless hydrothermal route in a small sealed autoclave containing 50 mL of equimolar solution of hexamethylenetetramine (HMTA, ≥99%, VWR, CAS-No 100-97-0) and zinc nitrate hexahydrate ($Zn(NO_3)2{\cdot}6H_2O$, 98%, Sigma-Aldrich, CAS-No 10196-18-6) at 25 mM and 90 °C for 4 h (Figure 1a). The flattened Zn wire substrate was kept vertically in the growth precursor solution during the growth duration. The Zn flat wire deposited was removed from the hydrothermal growth solution and thoroughly washed with distilled water before to be dried by a hot air flow (~30 s at ~53 °C). As-grown ZnO NSs were produced and compared to ZnO NSs post-annealed samples for 30 min at 350 °C. Samples were named ZnO/Zn(AG) and ZnO/Zn for as grown and post-annealed samples, respectively.

4.1.2. ZnO/Zn Sheets Production

The Zn roof sheet (5 cm × 5 cm) substrates were directly, without any washing process, functionalized by a one-step seedless hydrothermal route in sealed autoclave containing 300 mL of equimolar solution of HMTA and $Zn(NO_3)_2$ at 25 mM and 90 °C for 4 h (Figure 2a). The Zn roof sheet substrate was kept horizontally in the growth precursor solution during the growth duration. After 4 h, the Zn flat sheet functionalized was removed from the hydrothermal growth solution and thoroughly washed with DI water before to be dried by a hot air flow (~30 s at ~53 °C). Samples were named ZnO/Zn(AG).

4.2. ZnO/Zn Photocatalytic Activity Evaluation

4.2.1. Photodegradation under UV-Light

Photodegradation of MB was carried out under UV light irradiation (Hamamatsu LC-8, ~365 nm, $I_{received}$ by the sample ~35 mW/cm^2) with the aim to evaluate the best photocatalytic wire samples. Samples were immerged in 30 mL of an MB in DI water solution with an initial concentration of 10 µM placed under the UV source. After the light and the agitation were turned on, the photocatalysis process was monitored by UV–visible spectrophotometry (Perkin Elmer, Lambda 35) every 15 min for 3 h and the degradation efficiency X(%) was estimated using Equation (9):

$$X(\%) = \left(\frac{A_0 - A}{A_0}\right) \times 100 \quad (9)$$

where A_0 and A, respectively, stand for the initial and actual absorption peak values at the wavelength of the maximum absorption of MB (λ_{max} = 664 nm).

4.2.2. Photodegradation under Natural Solar Light

To prove the relevance of samples to answer to rainwater pollution under natural solar light, MB photocatalysis under natural solar light was carried out with ZnO NSs grown onto zinc wire samples. Experiments were realized at ambient temperature between April and May in Paris (France). Samples were immerged in 30 mL of an MB in DI water solution with an initial concentration of 10 µM. Every time, a beaker was filled with the dye solution and left without sample, to serve as a reference. The beakers were placed under natural solar light with an UV light intensity measured between 2.3 and 2.9 mW/cm^2, according to the weather. The photocatalytic process was monitored by UV–visible spectrophotometry every 30 min for 4 h. To confirm the sample efficiency in conditions closed to the real weather, the same experiments were carried out with a MB and AR14 solution in collected rainwater

(pH ~5.2) instead in DI water. The photodegradation efficiency X(%) was calculated using Equation (9) with λ_{max} equal to 664 nm for MB and 515 nm for AR14.

4.2.3. Polluted Runoff Water Photodegradation onto ZnO/Zn Sheets under Solar Light

To study the ZnO/Zn(AG) roof sheet photocatalytic efficiency in reproducible conditions, photodegradation of AR14 was carried out at the laboratory under an artificial solar lamp (Sirius-300 PU, Zolix, Beijing, China, 300 W, 320–2500 nm). The sample was placed under the solar light and a flow of polluted rainwater with AR14 at 10 µM has been imposed to simulate the runoff water comportment. The photocatalytic process was followed after one-pass of 10 mL of polluted rainwater with an imposed flow rate of 0.17–1.03 mL/min. Then, Equation (9) was used to calculate X(%). Between each experiment, called cycle, the sample was rinsed with DI water and replaced under the solar lamp for 15 min. After four cycles, the sample was used for two cycles more of water depollution without solar light irradiation of 15 min and with only DI water rinsing. The results showed a promising potential application of the functionalized Zn roof for water purification. By analogy with our previous work on ZnO NSs based photocatalytic construction materials [14,27], this kind of photocatalytic roof will be also performant for air purification.

5. Conclusions

Some building structures, especially roofs, have the potential to be used as very large photocatalytic reactors, exploiting sunlight to reduce urban pollution. In this context, Zn photocatalytic roof surfaces have been developed by a rapid one-step hydrothermal synthesis. This growth route is particularly attractive and efficient for growing ZnO NSs on a Zn surface, due to its cost effectiveness, ability to treat large areas, and ease of controlling chemical conditions. The resulting nanostructures are homogeneously distributed over the surface and exhibit good crystallinity. The post-annealing improved the ZnO NS crystallinity. The ZnO NSs have excellent photocatalytic properties under UV illumination for the degradation of MB. The photocatalytic activity of the functionalized ZnO/Zn has been demonstrated under solar light for the degradation of AR14 which is known to be less sensitive to photocatalysis under solar light. Finally, a runoff water purification experiment showed a real potential for application that can offer other environmental benefits, such as the removal of atmospheric pollutants, e.g., nitrogen oxides or organic volatile compounds.

Nevertheless, it is important to keep in mind that this study is still a primarily investigation. Therefore, more research work should be performed prior to using these functionalized roofs. The ZnO NSs should be tested for resistance in the acidic pH of water, dust deposition, and other climate factors. The Brunauer–Emmet–Teller (BET) method could be used to determine the specific surface area of the ZnO NSs. The photocatalytic activity of the aged samples should be evaluated in more depth and with real pollutants from rainwater.

Author Contributions: Manipulation realization, M.L.P. and A.P., conceptualization, Y.L.-W. and M.L.P.; methodology, M.L.P. and Y.L.-W.; validation, M.L.P. and Y.L.-W.; formal analysis, M.L.P., A.P., Y.L.-W., S.B. and M.D.; investigation, M.L.P. and Y.L.-W.; writing—original draft preparation, M.L.P. and Y.L.-W.; writing—review and editing, Y.L.-W., M.L.P., S.B. and M.D.; supervision, Y.L.-W. All authors have read and agreed to the published version of the manuscript.

Funding: This research received no external funding.

Acknowledgments: The authors want to thank M. Nicolas Hautiere from Gustave Eiffel University—COSYS Department for his advice to develop zinc-depolluting roof and his support.

Conflicts of Interest: The authors declare no conflict of interest.

References

1. Khayan, K.; Husodo, A.H.; Astuti, I.; Sudarmadji, S.; Djohan, T.S. Rainwater as a source of drinking water: Health impacts and rainwater treatment. *J. Environ. Public Health* **2019**, *2019*, 1760950. [CrossRef] [PubMed]
2. Fernando, L.T.D.; Ray, S.; Simpson, C.M.; Gommans, L.; Morrison, S. Remediation of fouling on painted steel roofing via solar energy assisted photocatalytic self-cleaning technology: Recent developments and future perspectives. *Adv. Eng. Mater.* **2022**, *24*, 2101486. [CrossRef]
3. Motamedi, M.; Yerushalmi, L.; Haghighat, F.; Chen, Z. Recent developments in photocatalysis of industrial effluents: A review and example of phenolic compounds degradation. *Chemosphere* **2022**, *296*, 133688. [CrossRef] [PubMed]
4. Marien, C.B.D.; Le Pivert, M.; Azaïs, A.; M'Bra, I.C.; Drogui, P.; Diarany, A.; Robert, D. Kinectics and mechanism of Paraquat's degradation: UV-C photolysis vs UV-C photocatalysis with TiO_2/SiC foams. *J. Hazard. Mater.* **2019**, *370*, 164–171. [CrossRef] [PubMed]
5. Tang, X.; Ughetta, L.; Shannon, S.K.; Houzé de L'aulnoit, S.; Hen, S.; Gould, R.A.T.; Russel, M.L.; Zhang, J.; Ban-Weiss, G.; Everman, R.L.A.; et al. De-pollution efficacy of photocatalytic roofing granules. *Build. Environ.* **2019**, *160*, 106058. [CrossRef]
6. Singh, V.P.; Sandeep, K.; Kushwaha, H.S.; Powar, S.; Vaish, R. Photocatalytic, hydrophobic and antimicrobial characteristics of ZnO nano needle embedded cement composites. *Construct. Build. Mater.* **2018**, *185*, 285–294. [CrossRef]
7. Zhang, X.; Li, H.; Harvey, J.T.; Liang, X.; Xie, N.; Jia, M. Purification effect on runoff pollution porous concrete with nano-TiO_2 photocatalytic coating. *Transport. Res. Part D* **2021**, *101*, 103101. [CrossRef]
8. Cerro-Prada, E.; Garcia-Salgado, S.; Quijano, M.A.; Varela, F. Controlled synthesis and microstructural properties of sol-gel TiO_2 nanoparticles for photocatalytic cement composites. *Nanomaterials* **2018**, *9*, 26. [CrossRef]
9. Bica, B.O.; Staub, J.V. Concrete blocks nano-modified with zinc oxide (ZnO) for photocatalytic paving: Performance comparison with tintanium dioxide (TiO_2). *Construct. Build. Mater.* **2020**, *252*, 119120. [CrossRef]
10. Liu, Y.; Kang, Z.H.; Shafiq, I.; Zapien, J.A.; Bello, I.; Zhang, W.J.; Lee, S.T. Synthesis, characterization, and photocatalytic application of different ZnO nanostructures in array configurations. *Cryst. Growth Des.* **2009**, *9*, 3222–3227. [CrossRef]
11. Asadi, S.; Hassan, M.M.; Kevern, J.T.; Rupnow, T.D. Development of photocatalytic pervious concrete pavement for air and storm water improvements. *J. Transport. Res. Board* **2012**, *2290*, 161–167. [CrossRef]
12. Guo, M.Z.; Ling, T.C.; Poon, C.S. Photocatalytic NO_x degradation of concrete surface layers intermixed and spray-coated with nano-TiO_2: Influence of experimental factors. *Cem. Concr. Compos.* **2017**, *83*, 279–289. [CrossRef]
13. Le Pivert, M.; Martin, N.; Leprince-Wang, Y. Hydrothermally grown ZnO nanostructures for water purification by photocatalysis. *Crystals* **2022**, *12*, 308. [CrossRef]
14. Le Pivert, M.; Zerelli, B.; Martin, N.; Capochihi-Gnambodoe, M.; Leprince-Wang, Y. Smart ZnO decorated optimized engineering materials for water purification under natural sunlight. *Const. Build. Mater.* **2020**, *257*, 119592. [CrossRef]
15. Baruah, S.; Dutta, J. Hydrothermal growth of ZnO nanostructures. *Sci. Technol. Adv. Mater.* **2009**, *10*, 013001. [CrossRef]
16. Demes, T.; Ternon, C.; Riassetto, D.; Stambouli, V.; Langlet, M. Comprehensive study of hydrothermally grown ZnO nanowires. *J. Mater. Sci.* **2016**, *51*, 10652–10661. [CrossRef]
17. Yu, Z.; Moussa, H.; Chouchene, B.; Schneider, R.; Wang, W.; Moliere, M.; Liao, H. Tunable morphologies of ZnO films via the solution precursor plasma spray process for improved photocatalytic degradation performance. *App. Surf. Sci.* **2018**, *455*, 970–979. [CrossRef]
18. Joshi, S.; Jones, L.A.; Sabri, Y.M.; Bhargava, S.K.; Sunkara, M.V.; Ippolito, S.J. Facile conversion of zinc hydroxide carbonate to Cao-ZnO for selective CO_2 detection. *J. Colloid Interface Sci.* **2020**, *558*, 310–322. [CrossRef] [PubMed]
19. Kumar, V.; Prakash, J.; Singh, J.P.; Chae, K.H.; Swart, C.; Ntwaeaborwa, O.M.; Swart, H.C.; Dutta, V. Role of silver doping on the defects related photoluminescence and antibacterial behaviour of zinc oxide nanoparticles. *Colloids Surf. B Biointerfaces* **2017**, *159*, 191–199. [CrossRef]
20. Chevalier-César, C.; Capochichi-Gnambodoe, M.; Lin, F.; Yu, D.; Leprince-Wang, Y. Effect of growth time and annealing on the structural defect concentration of hydrothermally grown ZnO nanowires. *AINS Mater. Sci.* **2016**, *3*, 562–572. [CrossRef]
21. Sun, Y.; Fuge, G.M.; Fox, N.A.; Riley, D.J.; Ashfold, M.N.R. Synthesis of Aligned Arrays of Ultrathin ZnO Nanotubes on a Si wafer coated with a thin ZnO film. *Adv. Mater.* **2005**, *85*, 2477–2481. [CrossRef]
22. Sun, Y.; Ndifor-Angwafor, G.N.; Riley, D.J.; Ashfold, M.N.R. Synthesis and photoluminescence of ultra-thin ZnO nanowire/nanotube arrays formed by hydrothermal growth. *Chem. Phys. Lett.* **2006**, *431*, 352–357. [CrossRef]
23. Sheng, Y.; Jiang, Y.; Lan, X.; Wang, C.; Li, S.; Liu, X.; Zhong, H. Mechanism and growth of flexible ZnO nanostructure arrays in a facile controlled way. *J. Nanomater.* **2011**, *2011*, 473629. [CrossRef]
24. Liu, B.; Zeng, H.C. Fabrication of ZnO "dandelions" via a modified kirkendall process. *J. AM. Chem. Soc.* **2004**, *126*, 16744–16746. [CrossRef]
25. Tak, Y.; Yong, K. Controlled growth of well-aligned ZnO nanorod array using a novel solution method. *J. Phys. Chem. B* **2005**, *109*, 19263–19269. [CrossRef]
26. Jung, S.H.; Oh, E.; Lee, K.-H.; Park, W.; Jeong, S.H. A sonochemical method for fabrication aligned ZnO nanorods. *Adv. Mater.* **2007**, *19*, 749–753. [CrossRef]
27. Le Pivert, M.; Kerivel, O.; Zerelli, B.; Leprince-Wang, Y. ZnO nanostructures based innovative photocatalytic road for air purification. *J. Clean. Prod.* **2021**, *318*, 128447. [CrossRef]

28. Cho, S.; Kim, S.; Jang, J.W.; Jung, S.H.; Oh, E.; Lee, B.R.; Lee, K.H. Large-scale fabrication of sub-20-nm-diameter ZnO nanorod arrays at room temperature and their photocatalytic activity. *J. Phys. Chem.* **2009**, *113*, 10452–10458. [CrossRef]
29. Bora, T.; Sathe, P.; Laxman, K.; Dobrestov, S.; Dutta, J. Defect engineered visible light active ZnO nanorods for photocatalytic treatment of water. *Catal. Today* **2017**, *284*, 11–18. [CrossRef]
30. Khoa, N.T.; Kim, S.W.; Thuan, D.V.; Yoo, D.H.; Kim, E.J.; Han, S.H. Hydrothermally controlled ZnO nanosheet self-assembled hollow spheres/hierarchical aggreagates and their photocatalytic activities. *CrystEngComm.* **2014**, *16*, 1344–1350. [CrossRef]
31. Akbal, F. Photocatalytic degradation of organic dyes in the presence of titanium dioxide under UV and solar light: Effect of operational parameters. *Environ. Prog.* **2005**, *24*, 317–322. [CrossRef]
32. Zinatloo-Ajabshir, S.; Heidari-Asil, S.A.; Salavati-Niasari, M. Recyclable magnetic ZnC2O4-based ceramic nanostructure materials fabricated by simple sonochemical route for effective sunlight-driven photocatalytic degradation of organic pollution. *Ceram. Intern.* **2021**, *47*, 8959–8972. [CrossRef]
33. Miao, J.; Lu, H.B.; Khiadani, D.; Kiadani, M.H.; Zhang, L.C. Photocatalytic degradatation of the Azo Dye Acid Red 14 in nanosized TiO2 suspension under simulated solar light. *Clean Soil Air Water* **2015**, *43*, 1037–1043. [CrossRef]